Photochemistry of CH_2BrCl: An ab Initio and Dynamical Study

Tamás Rozgonyi[†,‡] and Leticia González*[,§]

Institut für Optik und Quantenelektronik, Friedrich-Schiller-Universität Jena, Max-Wien-Platz 1, D-07743 Jena, Germany, and Institut für Chemie, Physikalische und Theoretische Chemie, Freie Universität Berlin, Takustrasse 3, D-14195 Berlin, Germany

Received: August 30, 2002

The photochemistry of CH_2BrCl has been studied using laser-induced wave packet propagations on coupled multistate CASPT2 potentials calculated for the electronic ground and low-lying excited states, as a function of two reaction coordinates corresponding to the two halogen eliminations. The results indicate that the lowest excited state, with character $^1(n\sigma^*)$, is strongly repulsive in both the C−Br and C−Cl directions. As a consequence, one-photon resonant excitation induces halogen fragmentation that occurs around 100 fs. The weaker C−Br bond dissociates directly, whereas the fragmentation of the stronger C−Cl bond involves a $n\sigma^*$(C−Br)/$n\sigma^*$(C−Cl) curve crossing pathway. The vertical spectrum for the resulting CH_2Br and CH_2Cl radicals has also been calculated, giving energies and oscillator strengths in close agreement with experimental UV spectral range and measured absorption cross-sections.

1. Introduction

Understanding the photochemistry of halomethanes has received significant attention in recent years for several reasons. First, these compounds are known to destroy stratospheric ozone[1] which makes them a popular target for tropospheric chemistry.[2−10] Second, they have been chosen as prototypes for mode specific photochemistry upon laser excitation, and therefore, a lot of questions have been raised regarding the mechanism by which preferential dissociation takes place.[11−22]

When halomethanes (in general CH_2XY species) absorb ultraviolet (UV) radiation, they are excited to various dissociative states where an electron is promoted from a lone pair orbital of the halogen to a carbon−halogen antibonding orbital: n(Y) → σ^*(C−Y). Halogen atoms and CH_2X radicals are then produced. In turn, the radicals are able to either photolyze again or recombinate. In this regard, chlorobromomethane, CH_2BrCl, is an interesting model because it can deliver bromine and chlorine atoms, as well as CH_2Br and CH_2Cl radicals into the earth's atmosphere. The Cl and Br atoms are both efficiently engaged in catalytic ozone depletion, where CH_2Br and CH_2Cl radicals are capable of releasing yet another halogen atom into the stratosphere. Because the atmospheric lifetimes of the halomethanes depend substantially on the photolytic destruction rates, it is logical to study their photodynamic behavior in order to assess their environmental impact.

Furthermore, because several dissociation paths are possible for halomethanes, numerous studies are aimed at observing bond selective dissociation upon light irradiation. Nowadays, controlling the outcome of a chemical reaction using pulsed light is an intriguing facet in the field of femtochemistry;[23] a cleverly shaped ultrashort laser pulse can find pathways which, without an external field, are either energetically forbidden or simply too inefficient.[24−26] In the early 80s, people thought it was enough to change the nature of the initial excitation to induce different dissociation pathways. For example, CH_2BrI photodissociated at 210 nm resulted in a bond-selective fragmentation of the C−Br bond rather than breaking the weaker C−I bond; on the contrary, excitations at 248 or 193 nm induced both fissions.[12,13] Recently it has been theoretically shown[21] that it is possible to control this branching ratio by means of coherent control, i.e., using constructive or destructive interference of coherent absorption pathways. As another theoretical model, C_2F_4IBr was used to control the branching ratio of I versus Br, upon 266, 248, and 193 nm excitations, but high selectivity was not observed.[15] State-resolved imaging for CF_2ClBr was also not selective: excitation at 234 nm produces a relative yield of 0.96 C−Br versus 0.04 C−Cl breaking.[20] In CH_2BrCl, experimental investigations at 248 and 234 nm showed exclusive C−Br dissociation,[8,16,19] whereas 193 nm or wavelengths around 200 nm achieved some C−Cl breaking.[10,11] So far, only femtosecond adaptive pulse shaping succeeded in really controlling C−Cl versus C−Br cleavage in CH_2BrCl.[22] However, this technique was used to maximize or minimize only the ion CH_2Br^+/CH_2Cl^+ ratio, which poses questions about whether the control is actually achieved in neutral or ionic surfaces.

Which pathway the system follows after a specific excitation is a question that has not yet been answered. The few models which have tried to understand the photodynamics in halomethanes indicate that the nonadiabatic curve crossing plays an important role.[8,10,15,17,18] Nevertheless, all available studies are based on simple model potentials for the n → σ^* excited states in the C−X and C−Y reaction coordinates, coupled by some arbitrary strength;[14,17,21] therefore, trends are difficult to generalize. In some studies, it is also suggested that the dissociation could involve Rydberg states that are then predissociated by ion-pair states.[22,27] In any case, the lack of potential energy surfaces for halomethanes prevents one from reaching firm conclusions.

Recently, we reported the vertical excitations of CH_2BrCl using the multistate-CASPT2 multiconfigurational method (MS−CASPT2).[28] Here it is of worth to remark that, as observed

* To whom correspondence should be addressed. E-mail: leti@chemie.fu-berlin.de.

† Institut für Optik und Quantenelektronik.

‡ Permanent address: Department of Spectr., Inst. of Isotope and Surface Chemistry, CRC, HAS, 1121 Budapest, Konkoly-Thege M. út 29-33., Hungary.

§ Freie Universität Berlin.

10.1021/jp026877x CCC: $22.00
Published on Web 10/24/2002

in previous studies, CASSCF or traditional single root CASPT2 approaches are not adequate for treating halomethanes because of strong Rydberg-valence mixing.[28] MS−CASPT2 predicted four valence states corresponding to either n(Br) → σ^*(C−Br) or n(Cl) → σ^*(C−Cl) transitions below the lowest Rydberg state, the first two in good agreement with the only available experimental UV spectrum measured by Orkin et al.[6] Encouraged by this preliminary study, we have computed potential energy curves for the ground and low-lying excited states in the C−Cl and C−Br coordinates, in an effort to understand the dissociation dynamics undergone after light irradiation. The electronic excitation energies of the resulting CH_2Br and CH_2-Cl radicals are also calculated, in good agreement with the latest experimental values. Furthermore, we have performed laser-driven wave packet propagations on coupled diabatic potentials, to estimate the dissociation times of CH_2BrCl. These calculations should draw light to the understanding of the photochemically initiated reactions occurring in the atmosphere and can also be used to gain insight into the laser control of bond breaking.

The paper is organized as follows. Section 2 presents the ab initio methods and the theory underlying the quantum dynamical simulations. In section 3, the UV spectra of the CH_2X radicals are established, the potential energy curves and transition dipole moments of CH_2BrCl are described, and the results of the laser-induced wave packet propagations are explained. Finally, section 4 summarizes the work.

2. Methodology

2.1. Ab Initio Quantum Chemistry. All calculations have been done within C_s symmetry, with the Br atom placed on the *z* axis and the Cl in the *xz* plane. As shown in ref 28, the nature of the transitions of A′ and A″ symmetry is very similar because of the near degeneracy of the molecular orbital lone pairs. Because most of the A′ excitations are more intense than the A″ counterparts, henceforth, we shall exclusively focuse on the A′ states. Moreover, because of the time scale in which dissociation takes place, intersystem crossing is not competitive and therefore, as a first approximation triplet states are not taken into account.

The potential energy curves for the electronic ground and low-lying singlet excited states of A′ symmetry and the corresponding transition dipole moments have been calculated using the equilibrium geometry of CH_2BrCl obtained at MP2-(fc)/6-311+G(d,p) level of theory.[28] The optimized parameters are r(C−Cl) = 1.764 Å, r(C−Br) = 1.933 Å, r(C−H) = 1.086 Å, θ(BrCCl) = 113.5°, θ(HCH) = 111.2°, and θ(HCBr) = 107.3°. For each reaction coordinate, the bond length C−Y (Y = Cl, Br) was varied over the range 1.6−10 Å, whereas the other geometrical parameters were kept fixed at their equilibrium values.

The electronic excited states of the dissociated molecules were determined at C−Y = 50 Å, for two different conformations: the nonrelaxed geometry, inherited from the original equilibrium geometry of CH_2BrCl, and the relaxed geometry of the corresponding CH_2X radicals. In the latter case, the equilibrium geometry optimized at the CCSD(T)/6-311++G(3df,3dp) level of theory was used.[29] Unlike the nonrelaxed geometries, both radicals have a planar structure in the electronic ground state. The optimized parameters reported in ref 29 are r(C−H) = 1.076 Å, r(C−Cl) = 1.696 Å, and θ(HCCl) = 117.8° for CH_2-Cl and r(C−H) = 1.075 Å, r(C−Br) = 1.851 Å, and θ(HCBr) = 117.9° for CH_2Br.

All of the excitation energies were obtained by means of multiconfigurational methods. Initially, the reference wave function and molecular orbitals were determined from a state average CASSCF (SA-CASSCF) calculation.[30] To recover the dynamical correlation this wave function is used in a subsequent multistate second-order perturbation theory treatment (MS−CASPT2).[31] The MS−CASPT2 approach uses a multidimensional reference space; that is, it couples simultaneously different single state perturbation theory solutions (SS−CASPT2 or simply CASPT2)[32] of the same symmetry previously included in the SA-CASSCF wave function. In this way, nearly degeneracies can be described and spurious Rydberg-valence mixings are removed. To eliminate intruder states, the level-shift technique has been used.[33] The level-shift was taken to be 0.3 au, unless stated otherwise. As described in ref 28, 11 roots of A′ symmetry are necessary to correctly describe the low-lying valence states of CH_2BrCl at the equilibrium geometry. At larger internuclear distances, Rydberg states disappear and nine roots suffice to describe the valence states. Therefore, from C−Y > 2.65 Å, nine roots have been used. This implies an energetic constant shift between the 11 and 9 root solution, which has been estimated and taken into account.

The active space used in the SA-CASSCF calculation consists of 12 electrons correlated in 12 orbitals, including the main σ,σ^*-(C−Y) orbitals, the nonbonding halogen *n* orbitals, and Rydberg orbitals. (For further details, see ref 28).

The following generally contracted basis sets of the atomic natural orbitals (ANO-L) were used for C, H, and Cl atoms:[34] (14s9p4d)/[4s3p2d] for the C atom, (8s4p)/[3s2p] for the H atoms, and (17s12p5d)/[5s4p2d] for the Cl atom. For the Br atom, the relativistic core potential AIMP (9s8p4d)/[3s4p2d] (effective atomic number $Z = 7.0$) was employed.[35] Additionally, the basis sets for C, Cl, and Br have been augmented with an extra set of 2s′2p′1d′ diffuse functions,[36] to evaluate Rydberg states.

The CASSCF state interaction method[37] was used to calculate the transition dipole moment functions d_{ij} from the corresponding perturbed-modified CAS (PMCAS) reference function,[31] that is, linear combinations of all CAS states involved in the MS−CASPT2 calculation. In the CH_2X radicals, where no Rydberg-valence mixing is present, the oscillator strength f is calculated as $2/3d_{ij}^2\Delta E$ using the energy differences ΔE obtained at the MS−CASPT2 level and d_{ij} estimated at the CASSCF level.

All of the MS−CASPT2/CASSCF calculations were carried out using the MOLCAS 5.0 quantum chemistry software.[38]

2.2. Quantum Dynamical Simulations. For simplicity, CH_2-BrCl is modeled as a pseudodiatomic with a dissociative bond q_Y = C−Y (Y = Cl, Br), whereas the rest of degrees of freedom are frozen and decoupled. This decoupling should be reasonable for ultrafast dissociation time scales because the energy remains in the dissociative bond and intramolecular vibrational redistribution can be neglected.

The simulation of the photodissociation dynamics is governed by the time dependent Schrödinger equation (TDSE), which can be written either in the adiabatic or diabatic representation.[39] In the adiabatic representation, the TDSE reads

$$i\hbar \frac{\partial \chi^{ad}(q_Y, t)}{\partial t} = \hat{H}^{ad}(q_Y, t)\, \chi^{ad}(q_Y, t) \qquad (1)$$

$\chi^{ad}(q_Y, t)$ is the nuclear wave function vector with the elements belonging to the corresponding electronic states and moving on the reaction coordinate q_Y under the action of the total adiabatic Hamiltonian $\hat{H}^{ad}(q_Y, t)$

$$\hat{H}^{ad}(q_Y, t) = \hat{H}^{ad}_{mol}(q_Y) - \underline{\underline{d}}^{ad}(q_Y)\underline{E}(t) \qquad (2)$$

The last term in eq 2 accounts for the interaction with the laser field $\underline{E}(t)$, where $\underline{\underline{d}}^{ad}(q_Y)$ represents the adiabatic transition dipole moment (TDM) matrix, whose elements are the adiabatic TDM vectors $\underline{d}_{ij}^{ad}$ between electronic states i and j.

The adiabatic molecular Hamiltonian $\hat{H}_{mol}^{ad}$ can be written as

$$\hat{H}_{mol}^{ad}(q_Y, t) = \hat{T}_n + \hat{K} + V^{ad}(q_Y) \tag{3}$$

In this representation, the potential matrix V^{ad} is diagonal containing the ith electronic potential energy curves $V_i(q_Y)$ as diagonal elements:

$$V^{ad}(q_Y) = \begin{pmatrix} V_1(q_Y) & 0 & \cdots \\ 0 & V_2(q_Y) & \\ \vdots & & \end{pmatrix} \tag{4}$$

and $\hat{T}_n$ is the nuclear kinetic energy operator with μ_Y being the corresponding reduced mass:

$$\hat{T}_n = -\frac{\hbar^2}{2\mu_Y}\frac{\partial^2}{\partial {q_Y}^2} \tag{5}$$

The nonadiabatic kinetic coupling term $\hat{K}$ is given by

$$\hat{K}_{ij} = -\frac{\hbar^2}{2\mu_Y}\left(2T_{ij}^{(1)}(q_Y)\frac{\partial}{\partial q_Y} + T_{ij}^{(2)}(q_Y)\right) \tag{6}$$

where $T_{ij}^{(1)}$ and $T_{ij}^{(2)}$ are defined in eq 7 being $\Phi_i(q_Y)$ the adiabatic electronic wave function corresponding to the ith adiabatic potential of $V^{ad}(q_Y)$:

$$T_{ij}^{(1)}(q_Y) = \left\langle \Phi_i(q_Y) \left| \frac{\partial}{\partial q_Y} \Phi_j(q_Y) \right\rangle \right. \tag{7a}$$

$$T_{ij}^{(2)}(q_Y) = \left\langle \Phi_i(q_Y) \left| \frac{\partial^2}{\partial {q_Y}^2} \Phi_j(q_Y) \right\rangle \right. \tag{7b}$$

Because the kinetic coupling is often rather sharply peaked if not singular when the wave function changes rapidly within a narrow space, it can cause numerical problems in the solution of the eq 1. An equivalent representation can be obtained by a unitary transformation U of the diagonal adiabatic potential matrix V^{ad} which gives the diabatic potential matrix V^d:

$$V^d = U^+ V^{ad} U \tag{8}$$

The same transformation must be applied to the adiabatic TDM matrix $\underline{\underline{d}}^{ad}(q_Y)$:

$$\underline{\underline{d}}^{d} = U^+ \underline{\underline{d}}^{ad} U \tag{9}$$

Assuming $T_{ij}^{(1)}$ is obtained, e.g., from ab initio calculations (see section 2.3), and knowing that U has to fulfill the differential equation[40]

$$\frac{\partial}{\partial q_Y} U + T^{(1)} U = 0 \tag{10}$$

it is possible to numerically estimate the U matrix.

Then, the TDSE in a diabatic representation can be expressed as

$$i\hbar \frac{\partial \chi^d(q_Y, t)}{\partial t} = \hat{H}^d(q_Y, t)\, \chi^d(q_Y, t) \tag{11}$$

where $\chi^d(q_Y, t)$ is the diabatic nuclear wave functions interconnected with the adiabatic one by

$$\chi^d(q_Y, t) = U^+ \chi^{ad}(q_Y, t) \tag{12}$$

and the diabatic Hamiltonian $\hat{H}^d$ is given by

$$\hat{H}^d(q_Y, t) = \hat{T}_n + V^d - \underline{\underline{d}}^d(q_Y)\, \underline{E}(t) \tag{13}$$

Now the kinetic coupling has been replaced by the potential coupling expressed by the off-diagonal terms $V_{ij}^d (i \neq j)$, which is indeed numerically easier to treat. In particular, eqs 1, with zero kinetic coupling, and 11, with nonzero potential coupling, have been both numerically solved using the split-operator scheme[41] and the fast Fourier technique,[42] with a time discretization of $\Delta t = 0.02$ fs.

The electric field $\underline{E}(t)$ is modeled as

$$\underline{E}(t) = \underline{E}_0 \cos(\omega t)\, S(t) \tag{14}$$

with amplitude $\underline{E}_0$, central frequency ω, and analytical shape function $S(t)$

$$S(t) = \sin^2(\pi t/t_p) \tag{15}$$

with pulse duration t_p.

Initially, we consider the molecule prepared in the vibrational ground state $\nu = 0$ of the electronic ground state $i = 0$

$$\chi(q_Y, t = 0) = \phi_{i\nu}(q_Y) = \phi_{00}(q_Y) \tag{16}$$

where χ stand for both the χ^{ad} and χ^d. The vibrational eigenfunctions $\phi_{i\nu}(q_Y)$ are evaluated using the Fourier Grid Hamiltonian method,[43] with a spatial grid of 2048 points.

2.3. Diabatization Procedure. The diabatic potentials and TDM are obtained from the adiabatic ones by calculating the transformation matrix U from eq 10. In principle, $T_{ij}^{(1)}$ can be evaluated directly by differentiating the wave function resulted from the ab initio calculations, but this requires a very dense grid of points in the potential energy curves. Instead, the diabatization procedure described in refs 44 and 45 has been applied. This involves approximating the kinetic coupling $T_{ij}^{(1)}$ with the help of an asymmetric Lorentzian function given by

$$T_{ij}^{(1)}(q) = \left\{ \begin{array}{ll} \dfrac{2\Gamma_{ij}^{l}}{4(q - r_{ij}^{c}) + (\Gamma_{ij}^{l})^2} \dfrac{2\Gamma_{ij}^{l}}{\Gamma_{ij}^{r} + \Gamma_{ij}^{r}} & \text{for } q \leq r_{ij}^{c} \\ \dfrac{2\Gamma_{ij}^{r}}{4(q - r_{ij}^{c}) + (\Gamma_{ij}^{r})^2} \dfrac{2\Gamma_{ij}^{r}}{\Gamma_{ij}^{l} + \Gamma_{ij}^{r}} & \text{for } q > r_{ij}^{c} \end{array} \right\} \tag{17}$$

where r_{ij}^c stands for the location of the crossing between the states i and j and Γ_{ij}^l and Γ_{ij}^r determine the half-widths of $T_{ij}^{(1)}(q)$ from the left and right-hand side of the crossing, respectively. The r_{ij}^c is determined from the analysis of the multiconfigurational wave function. The choice of $\Gamma_{ij}^{l,r}$ is based on the accurate matching of the diabatics with the adiabatics outside of the crossing region and on making the diabatics as smooth as possible in the crossing region.

3. Results and Discussion

3.1. CH_2Br and CH_2Cl Radicals. The UV absorption spectrum of the CH_2Br radical has been determined by Villenave and Lesclaux.[46] Using flash photolysis, they found a band

TABLE 1: MS−CASPT2 Calculated Excitation Energies ΔE (in eV), Corresponding Main Excitations and Oscillator Strengths f, for the CH_2X Radicals (X = Br and Cl)[a]

state	main excitation	ΔE	state	main excitation	ΔE	f
	Nonrelaxed CH_2Br Geometry			Relaxed CH_2Br Geometry		
a^2A''	$n_y(Br) \rightarrow \pi_x^*(C-Br)$	3.78	b^2A'	$\pi_x^*(C-Br) \rightarrow \sigma^*(C-Br)$	4.25 (4.45)[b]	0.0005
b^2A'	$\pi_x(C-Br) \rightarrow \pi_x^*(C-Br)$	4.26	a^2A''	$n_y(Br) \rightarrow \pi_x^*(C-Br)$	4.76 (4.80)	0.0000
c^2A'	$\pi_x^*(C-Br) \rightarrow \sigma^*(C-Br)$	4.78		$CH_2Br^+ + Cl^-$	4.98	0.0000
d^2A'	$\sigma(C-Br) \rightarrow \pi_x^*(C-Br)$	5.94	c^2A'	$\pi_x(C-Br) \rightarrow \pi_x^*(C-Br)$	5.38 (5.62)	0.0452
	Nonrelaxed CH_2Cl Geometry			Relaxed CH_2Cl Geometry		
a^2A''	$n_y(Cl) \rightarrow \pi_z^*(C-Cl)$	4.39	b^2A'	$\pi_z^*(C-Cl) \rightarrow \sigma^*(C-Cl)$	5.14 (5.23)	0.0004
b^2A'	$\pi_z(C-Cl) \rightarrow \pi_z^*(C-Cl)$	5.24	a^2A''	$n_y(Cl) \rightarrow \pi_z^*(C-Cl)$	5.19 (5.35)	0.0000
c^2A'	$\pi_z^*(C-Cl) \rightarrow \sigma^*(C-Cl)$	5.61		$CH_2Cl^+ + Br^-$	5.38	0.0000
	$CH_2Cl^+ + Br$	6.36	b^2A''	$\pi_z^*(C-Cl) \rightarrow \sigma^*(C-H)$	6.16	0.0000
b^2A''	$\pi_z^*(C-Cl) \rightarrow \sigma^*(C-H)$	7.21	c^2A'	$\pi_z(Cl-Cl) \rightarrow \pi_z^*(C-Cl)$	6.30 (6.51)	0.0459

[a] The left hand side are the results obtained for the nonrelaxed geometry of the CH_2X radical, whereas the right hand side corresponds to the relaxed geometry of CH_2X. In the case of the CH_2Cl radical a level-shift equal to 0.4 au was used. [b] In parentheses are the MRCI results calculated by Li and Francisco.[29]

peaking near 230 nm (5.39 eV), in disagreement with the spectrum previously reported by Nielsen et al.,[47] where two bands at 250 nm (4.96 eV) and 280 nm (4.43 ev) using the pulse radiolysis technique were detected. Villenave et al. claimed that the differences between the spectra are due to some secondary chemistry associated with the technique of pulse radiolysis and the weakness of the C−Br bond.[46] In solution, Chong et al.[48] have observed bands from transient resonance Raman spectroscopy with maxima below 220 nm, in both cyclohexane (using 239.5 nm excitation) and in methanol (239.5 and 228.7 nm excitation), which confirm the gas phase spectrum of Villenave and Lesclaux. On the theoretical side, though, calculations agree only qualitatively. Chong and co-workers[48] also performed time-dependent random phase calculations, which predict that the only singlet electronic absorption band of CH_2Br above 200 nm is located at 255 nm (4.86 eV) with an oscillator strength of $f = 0.0011$.[48] In contrast, MRCI/CASSCF(13,10) calculations from Li and Francisco[29] stated that the $2^2A'$ state located at 279 nm (4.45 eV) with $f = 0.08$ should be the one responsible for the absorption of CH_2Br in the atmosphere.

The spectrum of CH_2Cl has also been measured using flash photolysis by Roussel et al.[49] They showed that CH_2Cl has a maximum around 200 nm (6.2 eV).[49] Theoretically, the only calculations available are the MRCI from Li and Francisco[29] which assigned the experimental peak to the 1^2A_1 state at 237 nm (5.23 eV).

Table 1 shows our results calculated at the MS−CASPT2 level of theory. In the left-hand side, the results using the nonrelaxed geometries are presented, whereas the right-hand side corresponds to the excitations of the relaxed systems. For comparison, the results of Li and Francisco are also given.

Because we have performed the computation for the total $CH_2X + Y$ system, instead of computing the isolated CH_2X radical, there are degeneracies in the neutral dissociated channel. In fact, except for the ion-pair states, $CH_2X^+ + Y^-$, each state is three times degenerated, because the partially occupied p orbital of the cleaved halogen atom Y can have three linearly independent spatial orientations. These different orientations represent only rotations of the coordinates of the separated atom and do not influence the electronic configuration of the CH_2X radical in the dissociation limit. As a result, a global A′ state results in A′ and A″ symmetries in the radical. A global A″ symmetry calculation lead to exactly the same results. The ion-pair state is, nevertheless, unique and has A′ symmetry.

In the case of the CH_2Br radical, only four nondegenerate electronic excited states of global A′ symmetry are described within the first nine roots of the total system. The ionic dissociation channel in the ground-state $CH_2Br^+ + Cl^-$ is not present within the four low-lying excited states of the nonrelaxed geometry but appears as the third excited state for the relaxed geometry at 4.98 eV. This energy should be equal to the difference between the vertical ionization potential for the CH_2-Br radical (8.75 eV[50]) and the electron affinity of the Cl atom (3.613 eV[51]). This difference is 5.14 eV, in reasonable agreement with the calculated MS−CASPT2 value. The other three excited states correspond to the same valence states reported by Li and Francisco.[29] The outermost molecular orbital is an antibonding π orbital composed of the carbon 2p atomic orbital and the 3p atomic orbital of the halogen. In the $\pi_x^*(C-Br)$, the major contribution comes from the C atom, whereas in the $\pi_x(C-Br)$, it comes from the Br atom. For the sake of clarity, the corresponding excitations are schematically depicted in Figure 1.

As seen in Table 1, the first transition has a very low oscillator strength and the second one is forbidden. The fourth excited state, located at 5.38 eV, with character $\pi_x(C-Br) \rightarrow \pi_x^*(C-Br)$, possesses an oscillator strength of 0.0452, ca. 100 times bigger than the first excited state. The MRCI calculations, on the contrary, predict for the same state an $f = 1.53$, ca. 20 times stronger than the first state.[29] Such estimations would imply that the experimental spectrum should contain both bands or an onset of the second one at ca. 280 nm (cf. Table 1), in agreement with the bands observed by Nielsen et al.[47] Instead, MS−CASPT2 results (5.38 eV) are consistent with a single band peaking at 230 nm (5.39 eV) as reported by Villenave et al.[46]

From the measured absorption cross section, it is possible to fit a Gaussian in the frequency domain and then estimate the oscillator strength f as,[52]

$$f = \frac{1}{\pi r_e} \int \frac{\sigma(\lambda)}{\lambda^2} \, d\lambda \qquad (18)$$

where r_e is the classical electron radius ($r_e = 2.818 \times 10^{-6}$ nm) and $\sigma(\lambda)$ is the fitted absorption cross-section for each wavelength λ. As an approximation, the effect of line-broadening at room temperature is neglected. From the UV spectrum of CH_2Br measured by Villenave et al.,[46] we have estimated an $f = 0.0491$, in agreement with the MS−CASPT2 prediction; this corroborates that the CH_2Br radical does not absorb at wavelengths longer than 260 nm (4.77 eV),[46] and thus, its spectrum shows a single peak at 230 nm (5.39 eV).

The electronic excitations of CH_2Cl are also included in Table 1, together with the MRCI values of Li and Francisco.[29] The degeneracies allow us to calculate five excited electronic states.

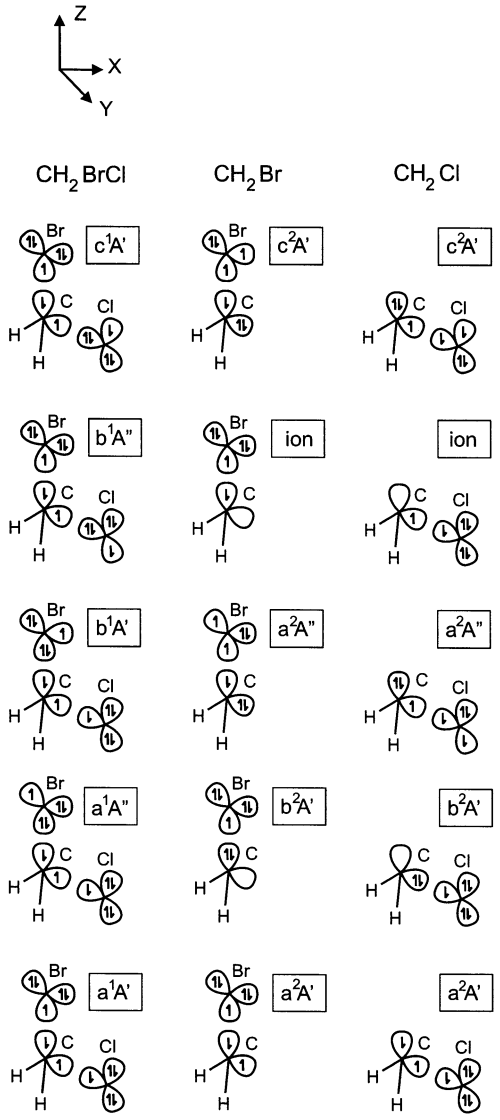

Figure 1. Electronic configurations of CH_2BrCl, CH_2Br, and CH_2Cl. Only the lone pairs of the halogen atoms (X = Br and Cl) and the σ,σ^* and π,π^* C−X orbitals are sketched in their corresponding orientations. The C−H orbitals are skipped for the sake of clarity; therefore, the b^2A'' state of CH_2Cl is not shown.

The ion-pair state appears as the third and fourth excited state in the relaxed and the nonrelaxed case, respectively. The difference between the vertical ionization potential of the CH_2-Cl radical (8.88 eV[50]) and the electron affinity of the Br atom (3.364 eV[51]) results in 5.516 eV, in acceptable agreement with the MS−CASPT2 value of 5.38 eV.

The electronic configurations of the first two excited states of the relaxed CH_2Cl radical, shown in Figure 1, are the same as those reported by Li and Francisco.[29] As in CH_2Br, the π_z^*(C−Cl) has a major contribution from the $2p_z$(C) and the π_z-(C−Cl) is dominated by the $3p_z$(Cl). It is interesting to note that the transition energies obtained through the MRCI approach are overestimated with respect to the MS−CASPT2 excitation energies. This general trend has been already observed and discussed for some organometallic complexes.[53] The transition π_z^*(C−Cl) → σ^*(C−H), which is in the present work the third singlet excited state of the neutral radical, is missing in ref 29. This transition has a zero oscillator strength, as well as the second excitation, n_y(Cl) → π_z^*(C−Cl). Again, the first transition for the relaxed radical has a low oscillator strength, ca. 100 times weaker than the fourth excited state. Hence, the first peak in the experimental spectrum measured at 200 nm (6.20 eV)[49] should be assigned to the π_z(C−Cl) → π_z^*(C−Cl) transition (c^2A' state), located by MS−CASPT2 at 6.30 eV (197 nm) with an oscillator strength of 0.0459. Because the measured data[49] did not allow an accurate fit, especially in the low wavelength region, eq 18 predicts presumably an overestimated oscillator strength of $f = 0.0852$, yet closer to the MS−CASPT2 value (cf. Table 1) than to the MRCI value of 1.47 reported in Ref 29.

TABLE 2: MS−CASPT2 Calculated Excitation Energies ΔE (in eV), Corresponding Main Excitations and Oscillator Strengths f, for the CH_2BrCl Molecule in the Equilibrium Geometry (Adapted from Ref 28)

state	main excitation	ΔE (eV)	f
a^1A''	n_y(Br) → σ^*(C−Br)	6.04	0.0078
b^1A'	n_x(Br) → σ^*(C−Br)	6.12	0.0071
b^1A''	n_y(Cl) → σ^*(C−Cl)	7.11	0.0049
c^1A'	n_z(Cl) → σ^*(C−Cl)	7.17	0.0207
c^1A''	n_y(Br) → Rydb.A′	7.40	0.0442
d^1A'	n_x(Br) → Rydb.A′	7.42	0.0385
e^1A'	n_z(Cl) → σ^*(C−Br)	7.79	0.0023
d^1A''	n_y(Cl) → σ^*(C−Br)	7.86	0.0014
f^1A'	n_z(Cl) → Rydb.A′	8.15	0.0233
e^1A''	n_x(Br) → Rydb.A″(1)	8.17	0.0010
g^1A'	n_y(Br) → Rydb.A″(1)	8.19	0.0033
f^1A''	n_y(Cl) → Rydb.A′	8.22	0.0009
g^1A''	n_y(Br) → σ^*(C−Cl)	8.48	0.0024
h^1A'	n_x(Br) → σ^*(C−Cl)	8.59	0.1567
h^1A''	n_z(Cl) → Rydb.A″(1)	9.05	0.0006
i^1A'	n_y(Br) → Rydb.A″(2)	9.09	0.0349
i^1A''	n_x(Br) → Rydb.A″(2)	9.16	0.0166
j^1A'	n_y(Cl) → Rydb.A″(1)	9.16	0.0003
j^1A''	n_z(Cl) → Rydb.A″(2)	9.83	0.0047
k^1A'	n_y(Cl) → Rydb.A″(2)	9.88	0.0002

3.2. CH_2BrCl Potential Energy Curves. *3.2.1. Vertical Spectrum and Adiabatic Potentials.* The electronic configuration of CH_2BrCl in the electronic ground state conforms to a closed shell $^1A'$ state corresponding to σ(C−Cl)$^2\sigma$(C−Br)^2 n_z(Cl)^2 n_x-(Br)^2 n_y(Cl)^2 n_y(Br)$^2\sigma^*$(C−Cl)$^0\sigma^*$(C−Br)^0.

Table 2 summarizes the low-lying excitations of the parent molecule pictorially shown in Figure 1. According to the MS−CASPT2 calculations, in both symmetries, two valence states are found below the first Rydberg transition. They correspond to the transitions n(Br) → σ^*(C−Br) calculated at 6.1 eV (203 nm) and n(Cl) → σ^*(C−Cl) lying at 7.2 eV (173 nm). According to Orkin et al.,[6] the experimental UV spectrum of CH_2BrCl has a maximum cross-section at 202.6 ± 0.5 nm (6.1 eV) which according to the MS−CASPT2 results can be assigned to n(Br) → σ^*(C−Br) transitions. From the measured spectrum[6] the estimated oscillator strength belonging to this peak from eq 18 is $f = 0.0126$. Because the excitation energies to the bA′ and aA″ states lie very close to each other, the measurement cannot resolve these two transitions; thus, the value of f should correspond roughly to the sum of our oscillator strengths 0.0071 (*bA′*) and 0.0078 (*aA″*), i.e., to 0.0149. Although the effect of the temperature (298 K) at which the spectrum was measured is ignored here, the computed oscillator strength agrees well with the one deduced from the measured spectrum, confirming the assignment. Unfortunately, no absorption cross sections were measured below 187 nm, but the experimental absorption profile shows an increasing tendency starting at 192 nm, which according to our results must correspond to the onset of the n_z(Cl) → σ^*(C−Cl) absorption band.

The four lowest A′ adiabatic potential energy curves along the C−Br and C−Cl bonds together with cubic splines fitted to the ground and first two electronic excited states are shown in Figure 2. To get a better insight at short internuclear distance,

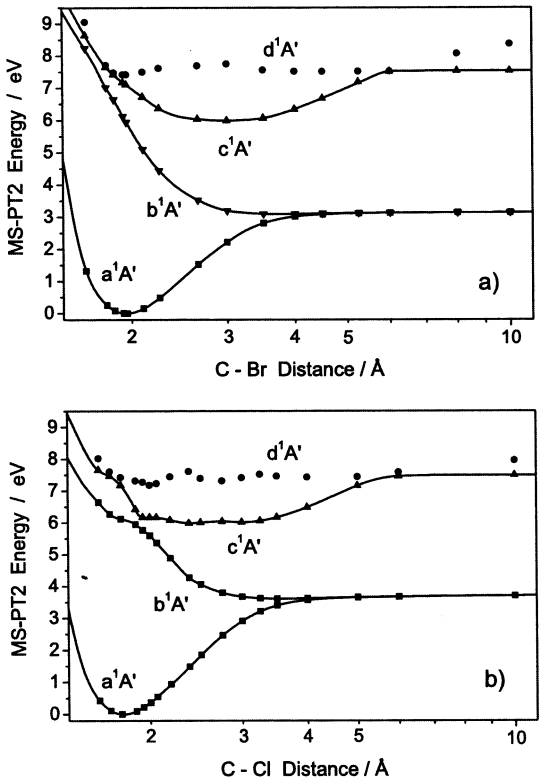

Figure 2. MS−CASPT2 adiabatic potential energy curves along C−Br (a), and C−Cl (b) directions, with *x* axis in logarithmic scale (Å). Cubic splines are shown in solid lines.

the horizontal axis is logarithmic. Along the C−Cl bond, a level shift LS = 0.3 au ensured reliable CASSCF reference weights and converged MS−CASPT2 correlated energies. In the C−Br direction, LS = 0.4 au for C−Br > 3 Å was used. Only this higher LS value achieves reliable CASSCF reference weights and obtains the real energy of the diabatic state belonging to the transition $n_y(Cl) + n_y(Br) \rightarrow \sigma^*(C-Br)$, which appears as the ninth root at around C−Br = 2.5 Å and correlates to the first excited state $n_y(Cl) \rightarrow \pi_z^*(C-Cl)$ of the CH_2Cl radical for its nonrelaxed geometry.

As expected from the analysis of the vertical spectrum of the parent molecule (cf. Table 2), the first adiabatic excited state is directly dissociative in the C−Br direction (see Figure 2a). On the other hand, this state is also dissociative in the C−Cl direction, because of an avoided crossing between the c^1A' and the b^1A' states. Nevertheless, the adiabatic state b^1A' is less steep in the C−Cl direction than in the C−Br one, indicating preferential C−Br bond fission after excitation to the first electronic excited state, in agreement with experimental observations.[16,19]

From Figure 2, we see that the second *adiabatic* excited state (c^1A') is bound in both directions. However, two things should be kept in mind to understand the real photodynamics occurring in this state: (i) the nonadiabatic coupling with other potentials (see section 3.2.2) and (ii) the fact that the present potentials are only one-dimensional and nonrelaxed. In addition, it is known that the first electronic excited states of both CH_2Cl and CH_2Br radicals are strongly dissociative for the halogen atom.[29] This suggests that the c^1A' adiabatic potential is open for the $CH_2BrCl \rightarrow CH_2 + Br + Cl$ dissociation. We have computed the ground-state energy for C−Br = C−Cl = 10 Å distances using the nonrelaxed geometry and MS−CASPT2 predicts 7.18 eV with respect to the ground-state energy of the CH_2BrCl equilibrium geometry, i.e., the same as the vertical excitation

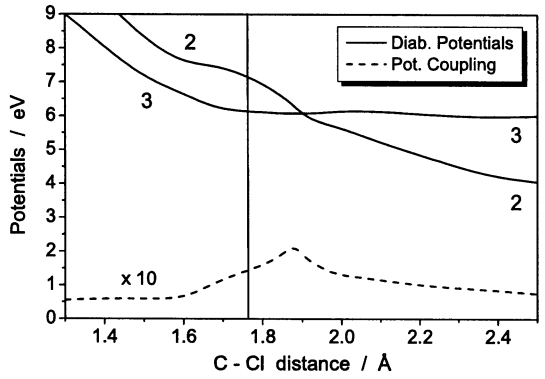

Figure 3. Diabatized potentials in the vicinity of the crossing located at C−Cl = 1.9 Å. The diabatic states are indicated by the indices *j*. The dashed line represents the potential coupling $V_{23}(R)$ multiplied by a factor 10 for better visualization. The ground-state equilibrium C−Cl distance is indicated by the vertical line.

energy of the c^1A' state for the CH_2BrCl (see Table 2). Considering geometry-relaxation, this computation supports the possibility of $CH_2BrCl \rightarrow CH_2 + Br + Cl$ dissociation.

From the vertical excitation energies of the CH_2BrCl in its equilibrium geometry and the energies of its radicals, the dissociation energies in the electronic ground state can be computed.[54] For nonrelaxed CH_2X radicals, the dissociation energies in the C−Br channel are 3.22[55] and 3.71 eV for the C−Cl channel. The dissociation energies computed using the relaxed geometries are 2.99 and 3.47 eV for the C−Br and C−Cl channels, respectively; these are very close to the experimental values for the dissociation energies of CH_2Cl-Br and CH_2Br-Cl which are 285 (2.95) and 331 kJmol^{-1} (3.43 eV), respectively.[19,16] The differences between dissociation energies belonging to the nonrelaxed ground state potentials and the values obtained for relaxed radicals are about 0.23 eV in both channels. These differences will not influence the dissociation dynamics as long as dissociation into the electronic ground state of the radicals is considered, i.e., as long as the molecule is dissociated in the first excited electronic state. Excitation energies and electronic configurations, however, strongly depend on the geometry of the radical, as shown in section 3.1.

3.2.2. Diabatic Potentials. To understand how the photoproducts CH_2X are formed, the crossings between the c^1A' and b^1A' excited states, corresponding to $n_z(Cl) \rightarrow \sigma^*(C-Cl)$ and $n_x(Br) \rightarrow \sigma^*(C-Br)$ transitions in the Franck−Condon (FC) region, need to be investigated. The first crossing along the C−Cl coordinate takes place at around C−Cl = 1.90 Å, and at this point, the corresponding separation is 0.37 eV. This is the only crossing we have diabatized for it is the crucial point to understand the nonadiabatic population transfer.[17]

The diabatized potentials are shown in Figure 3, together with the potential coupling. Using numerical indices for the diabatic curves, the diabatization parameters are: $\Gamma^l_{23} = 0.08$, $\Gamma^r_{23} = 0.10$, $r^c_{23} = 1.89$, and $\hat{r}^c_{23} = 1.90$. The $\hat{r}^c_{23}$ value is the real crossing point, which differs from r^c_{23} because of the asymmetric nature of Lorentzian. The choice of these parameters is justified in view of the fact that small changes do not affect the population dynamics described in section 3.3.

Although a complete diabatization was not performed, an analysis of the multiconfigurational wave function provides us with a scheme of the diabatics which contribute to the b^1A' and c^1A' adiabatic curves. This is presented in Figures 4 and 5 for the C−Cl and C−Br reaction coordinates, respectively.

Let us first investigate the potential curves in the C−Cl direction. As shown in Figure 4, two diabatics contribute to

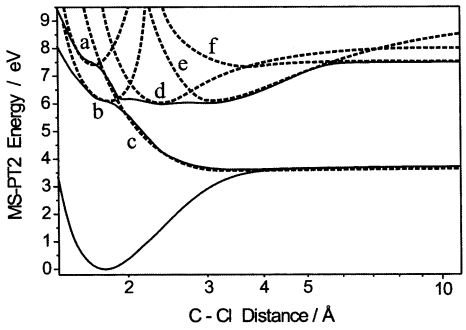

Main configurations of the diabatic potentials:	
a :	$n_x(\mathrm{Br}) \rightarrow Rydb.\ A'$
b :	$n_x(\mathrm{Br}) \rightarrow \sigma^*(\mathrm{C-Br})$
c :	$n_z(\mathrm{Cl}) \rightarrow \sigma^*(\mathrm{C-Cl})$
d :	$n_x(\mathrm{Br}) \rightarrow \sigma^*(\mathrm{C-Cl})$
e :	$\sigma(\mathrm{C-Cl}) \rightarrow \sigma^*(\mathrm{C-Cl})$
f :	$n_y(\mathrm{Cl})+n_y(\mathrm{Br}) \rightarrow \sigma^*(\mathrm{C-Cl})$

Figure 4. Schematic picture of the diabatic states (dashed) which contribute to the lowest two excited adiabatic potentials (solid) along the C−Cl coordinate. The *x* axis is in logarithmic scale.

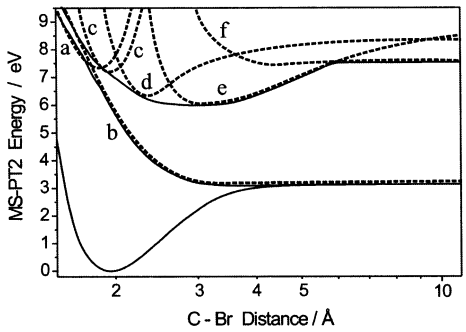

Main configurations of the diabatic potentials:	
a :	$n_x(\mathrm{Br}) \rightarrow Rydb.\ A'$
b :	$n_x(\mathrm{Br}) \rightarrow \sigma^*(\mathrm{C-Br})$
c :	$n_z(\mathrm{Cl}) \rightarrow \sigma^*(\mathrm{C-Cl})$
d :	$n_z(\mathrm{Cl}) \rightarrow \sigma^*(\mathrm{C-Br})$
e :	$\sigma(\mathrm{C-Br}) \rightarrow \sigma^*(\mathrm{C-Br})$
f :	$n_y(\mathrm{Cl})+n_y(\mathrm{Br}) \rightarrow \sigma^*(\mathrm{C-Br})$

Figure 5. Schematic picture of the diabatic states (dashed) which contribute to the lowest two excited adiabatic potentials (solid) along the C−Br coordinate. The *x* axis is in logarithmic scale.

the first adiabatic excited state, b^1A'. These are the $n_x(Br) \rightarrow \sigma^*(C-Br)$ and $n_z(Cl) \rightarrow \sigma^*(C-Cl)$ denoted by b and c in the figure. This crossing is critical for the wave packet dynamics in the second adiabatic excited state, c^1A'. The adiabatic curve c^1A' is formed by several diabatics. In the FC region, it is determined by the diabatic c, which correlates with the ground state of the dissociation products, CH_2Br and Cl. Before the FC region, the cA′ is determined by the lowest Rydberg state, $n_x(Br) \rightarrow$ Rydb.A′, denoted by a in the figure. Just after the FC region, another crossing occurs between diabatic b and d, the later referring to the configuration $n_x(Br) \rightarrow \sigma^*(C-Cl)$, which is the seventh excited state of symmetry A′ at equilibrium geometry (see Table 2). This diabatic state correlates with the second excited state $\pi_x(C-Br) \rightarrow \pi_x^*(C-Br)$ of the CH_2Br fragment in the nonrelaxed dissociation limit (cf. Table 1). The last two contributions come from the diabatic states e and f. The former corresponds to the configuration $\sigma(C-Cl) \rightarrow \sigma^*(C-Cl)$ correlating with the ionic dissociation channel, $CH_2Br^+ + Cl^-$. The latter is a double excitation of the parent molecule from the two lone pair orbitals of A″ symmetry of the halogen atoms, i.e., $n_y(Cl) + n_y(Br) \rightarrow \sigma^*(C-Cl)$; it correlates in the nonrelaxed dissociation limit with the first excited state of the CH_2Br radical, i.e., with $n_y(Br) \rightarrow \pi_x^*(C-Br)$. The extremely small energy gap between curves e and f in the vicinity of the crossing (between 5.6 and 5.8 Å) suggests that this crossing is rather nonavoided, indicating a very low probability of population transfer from one *diabatic* curve to the other.

The diabatic contributions to the adiabatic potentials along the C−Br bond show strong similarities with the diabatic structure already discussed. Curves a, b, and c in Figure 5 are the same electron configurations as those in Figure 4. Likewise, the adiabatic states d, e, and f in the C−Br direction are the counterparts to those in the C−Cl direction. This means that Figure 5 refers to the following electron configurations: (i) state d possesses $n_z(Cl) \rightarrow \sigma^*(C-Br)$ character, correlating with the second excited state of the nonrelaxed CH_2Cl fragment in the dissociation limit; (ii) state e denotes the transition $\sigma(C-Br) \rightarrow \sigma^*(C-Br)$ correlating with the ion-pair channel, $CH_2Cl^+ + Br^-$; and (iii) state f is $n_y(Cl) + n_y(Br) \rightarrow \sigma^*(C-Br)$ and correlates with the first excited state of the nonrelaxed CH_2Cl fragment, $n_y(Cl) \rightarrow \pi_z^*(C-Cl)$. Again, the crossing between e and f at C−Br ≈ 6 Å should be not avoided because the energy difference at this point is less than 0.013 eV.

3.2.3. Transition Dipole Moments. The nonzero components (*x* and *z*) of the transition dipole moment vectors between the first two adiabatic excited states of symmetry A′ and the ground state are presented in Figure 6. In each figure, the FC transition is indicated by a vertical line.

As already pointed out by the oscillator strengths obtained at the equilibrium geometry (cf. Table 2), the $a^1A' \rightarrow c^1A'$ transition is considerably stronger than the $a^1A' \rightarrow b^1A'$ one. According to Figure 6, this trend persists along the reaction path. In both directions, the TDM of the $a^1A' \rightarrow b^1A'$ transition takes its maximum value close to the FC region, and it is parallel to the *Z* axis, i.e., to the C−Br bond, indicating that the transition to the first excited state is parallel.

The maxima of the TDM curves are due to the state crossings. The peak of the *z* component of the TDM in the $a^1A' \rightarrow b^1A'$ transition along the C−Br distance (cf. Figure 6a) indicates the crossing between the diabatics a and b, shown in Figure 5. Similarly, the maximum of the TDM in Figure 6b is the result of the crossing between diabatics e and d (see Figure 5). In the C−Cl direction, the peak of both TDM components for the $a^1A' \rightarrow b^1A'$ transition is located at ca. C−Cl = 1.9 Å, (cf. Figure 6c) confirming the crossing between the diabatics b and c (cf. Figure 4). The smaller local maxima of *x* and *z* components of the $a^1A' \rightarrow c^1A'$ transition along the C−Cl direction around the equilibrium geometry reflect the crossing between diabatics a and c displayed in Figure 4. Likewise, the overall maximum shown in Figure 6d, at C−Cl = 3 Å, is due to the crossing between diabatics e and d at around C−Cl = 2.8 Å (see Figure 4). In conclusion, the shape of the TDM curves confirms the diabatics proposed by analyzing the electronic configurations displayed in Figures 4 and 5.

The diabatized TDM in the C−Cl coordinate are shown in Figure 7. Note that the diagonal elements of the adiabatic TDM

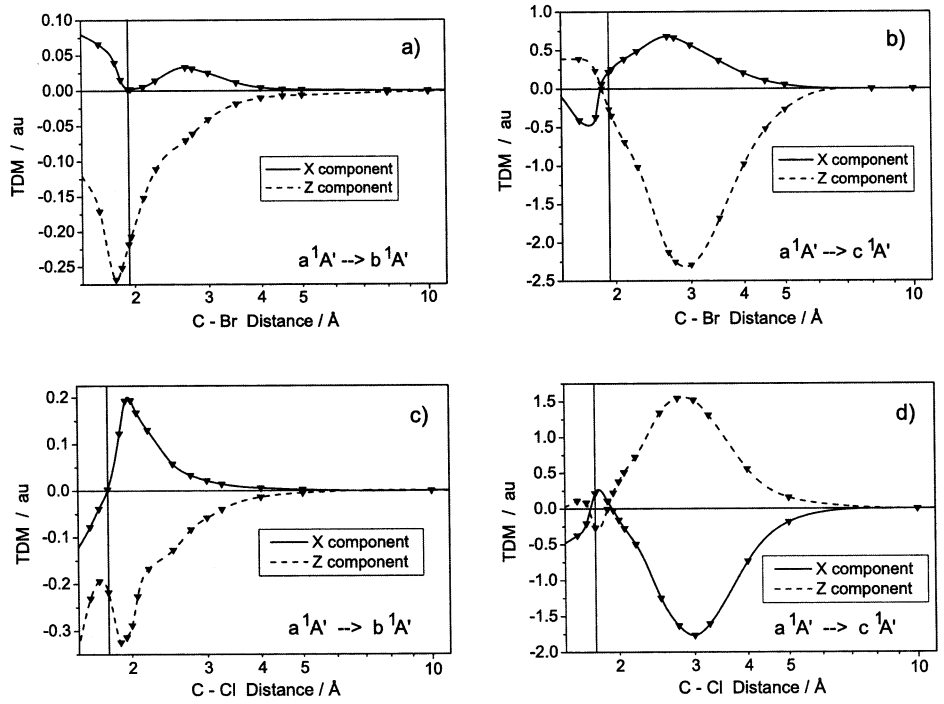

Figure 6. Adiabatic transition dipole moments as a function of C−Br distance for transitions aA′ → bA′ and aA′ → cA′. Panels a and b display the TDM components along the C−Br coordinate, whereas c and d display the TDM components along the C−Cl coordinate. Solid and dashed lines belong to *x* and *z* components of the TDM, respectively. The *C*−*X* axis is scaled logarithmic.

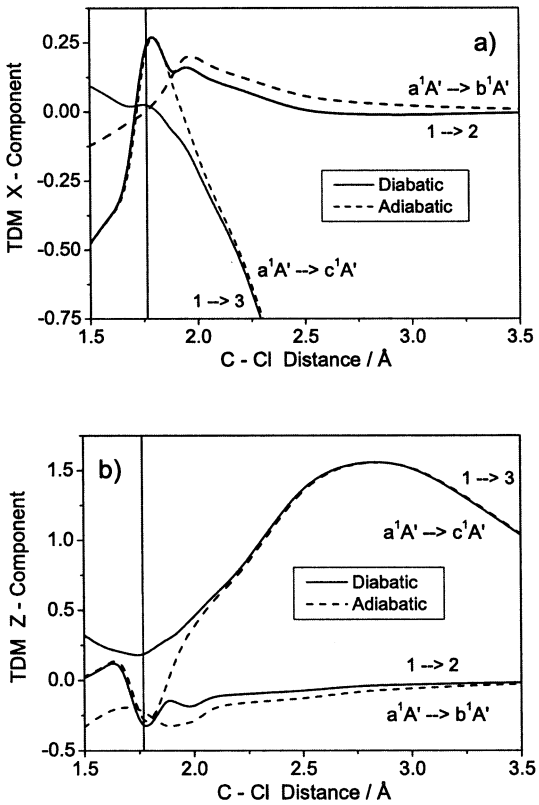

Figure 7. Diabatized transition dipole moment curves (solid) and adiabatic ones (dashed). The ground-state equilibrium C−Cl distance is indicated by a vertical line.

matrix were set to zero, because they do not play a role in UV excitations. Also, the off-diagonal elements $\underline{d}_{23}^{\mathrm{ad}}$ coupling b^1A' and c^1A' excited states were ignored, because the photon energies of the present investigations do not match the transition energy between these states.

3.3. Quantum Dynamical Simulations. Here, we focus on studying the dissociative lifetimes of CH_2BrCl using molecular wave packet simulations in the two low-lying excited states. The validity of the present one-dimensional approximation is restricted to those cases where the potential gradient is steeper in one direction than in the other one at the FC region and almost exclusive dissociation along a particular channel is expected; that is, along the C−Br coordinate the b^1A' state is steeper than along the C−Cl one and the reverse is true in the c^1A' state (see Figure 2).

In principle, to extract the lifetime of the system, it is generally enough to assume that the molecule is photoexcited by a δ pulse of infinitesimal duration δt.[56] In that case, the wave packet at its start in the upper state equals the initial wave function of the parent molecule multiplied by the transition dipole function.[57] For a more realistic case than an ideal δ-pulse excitation, specially when crossings are involved, real laser pulses with a finite duration are needed. In addition, working with real pulses offers the advantage that they serve as a preliminary basis to enlighten more complicated laser-driven experiments in CH_2XY molecules. Therefore, we shall use ultrashort laser pulses which induce a one-photon resonant transition in either the b^1A' or c^1A' states. The laser pulse thus drives the system from the electronic ground state to some excited state, from where population may be transferred to other excited states via nonadiabatic coupling. The population of the excited state *j* is given by $P_j(t)$

$$P_j(t) = \int_0^{\infty} |\chi_j(q_Y, t)|^2 \, \mathrm{d}q_Y \qquad (19)$$

where χ_j may refer either to diabatic state χ_j^{d} or adiabatic state χ_j^{ad}, depending on which representation is used.

Likewise, the probability of dissociation, which indicates which fraction of the wave packet has passed a certain bond

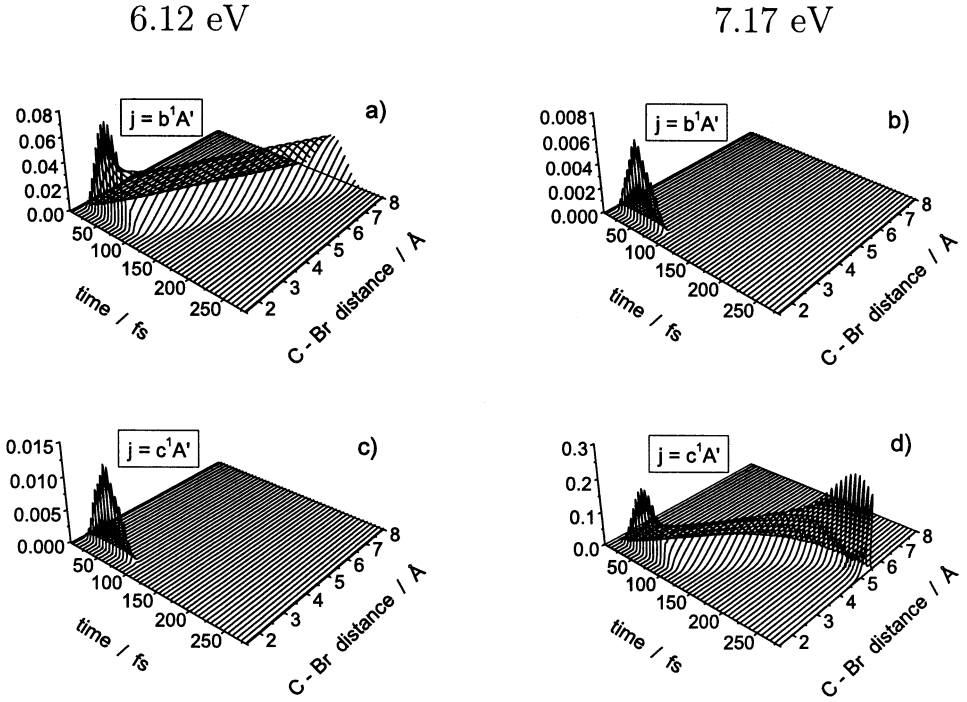

Figure 8. Propagation of one-dimensional wave functions, $|\chi^{ad}_{j\epsilon=z}(q_{Br}, t)|$ on adiabatic potential curves $j = b^1A'$, c^1A' under irradiation with a pulse of $t_p = 100$ fs duration and photon energy of 6.12 (l.h.s) or 7.17 eV (r.h.s).

distance b in the excited state j, at time t, is described by $P_{diss,j}(t)$

$$P_{diss,j}(t) = \int_b^\infty |\chi_j(q_Y, t)|^2 \, dq_Y \tag{20}$$

The boundary value b, separating the interaction ($q_Y \leq b$) from the asymptotic domains ($b \leq q_Y$) of the potentials, was estimated 6 Å for both directions.

Because the TDM corresponding to the A′ states possess two components, x and z, it is possible to photoexcite the wave packet of the fixed molecule with x- or z-linearly polarized light (see eq 2). This is equivalent to consider a uniform distribution of molecule orientations and, therefore, perform a classical averaging over the molecular orientations by averaging the effects of the three different possible polarization directions of light, ϵ. The average population $\overline{P_j(t)}$ can be then written as[56]

$$\overline{P_j(t)} = \overline{P_{jx}(t)} + \overline{P_{jz}(t)} \tag{21}$$

where

$$\overline{P_{j\epsilon}(t)} = \frac{1}{3}\int_0^\infty |\chi_{j\epsilon}(q_Y, t)|^2 \, dq_Y \tag{22}$$

The $\chi_{j\epsilon}(q_Y, t)$ is the solution of either eq 1 or 11 under the condition that the electric field $\underline{E}$ is polarized in the ϵ direction.

Similarly, the average probability of dissociation $\overline{P_{diss,j}(t)}$ is obtained by[56]

$$\overline{P_{diss,j}(t)} = \overline{P_{diss,jx}(t)} + \overline{P_{diss,jz}(t)} \tag{23}$$

where

$$\overline{P_{diss,j\epsilon}(t)} = \frac{1}{3}\int_b^\infty |\chi_{j\epsilon}(q_Y, t)|^2 \, dq_Y \tag{24}$$

If the dissociation takes place in one step, the corresponding $\overline{P_{diss}(t)}$ curves can be usually very well fitted by the following sigmoid function:

$$\overline{P_{diss}(t)} = \overline{P_{diss}} \, [1 + e^{-(t-t'_{diss})/Dt}]^{-1} \tag{25}$$

where the parameter Dt is mainly determined by the length of the pulse, $\overline{P_{diss}}$ is the asymptotic dissociation probability, and t'_{diss} is the time at which $\overline{P_{diss}(t)}$ takes the half of its maximum value, $\overline{P_{diss}}$. This moment can be taken as the "absolute" time of the dissociation. In the case of a pulse with energy density far below the saturation energy density and centered at time t_0, the dissociation time t_{diss} can be defined as

$$t_{diss} = t'_{diss} - t_0 \tag{26}$$

3.3.1. Laser-Induced Wave Packet Propagations. We use photon energies of 6.12 or 7.17 eV corresponding to the transition energies of $a^1A' \rightarrow b^1A'$ and $a^1A' \rightarrow c^1A'$ transitions, respectively (see Table 2). In passing, we note that 6.2 eV is directly accessible with four photons of 800 nm, which is the standard wavelength of the commercial femtosecond laser systems, whereas reaching the c^1A' state would need five photons. The rest of the pulse parameters are $t_p = 100$ fs (equivalent to 36.4 fs at fwhm in intensity), $t_0 = 50$ fs, and $E_0 = 0.5$ GVm^{-1} (0.033 TWcm^{-2} peak intensity). These pulse parameters were chosen somewhat arbitrarily under the conditions that the duration of the pulse is shorter than the dissociation times and the pulse energy is far below the saturation energy. Simulations have been performed using noncoupled adiabatic potentials for the C−Br and coupled potentials for the C−Cl coordinate.

The propagation of the wave packets $\chi_{j\epsilon}(q_Y, t)$ in each C−Y direction under both selected photon energies is shown in Figures 8 and 9 for Y = Br and Y = Cl, respectively. Because the use of an electric field parallel to the x and to the z components of the TDM vector mainly influences the amount of transferred population but not the dynamical behavior, only the results using z-polarized light are shown. Along the C−Br

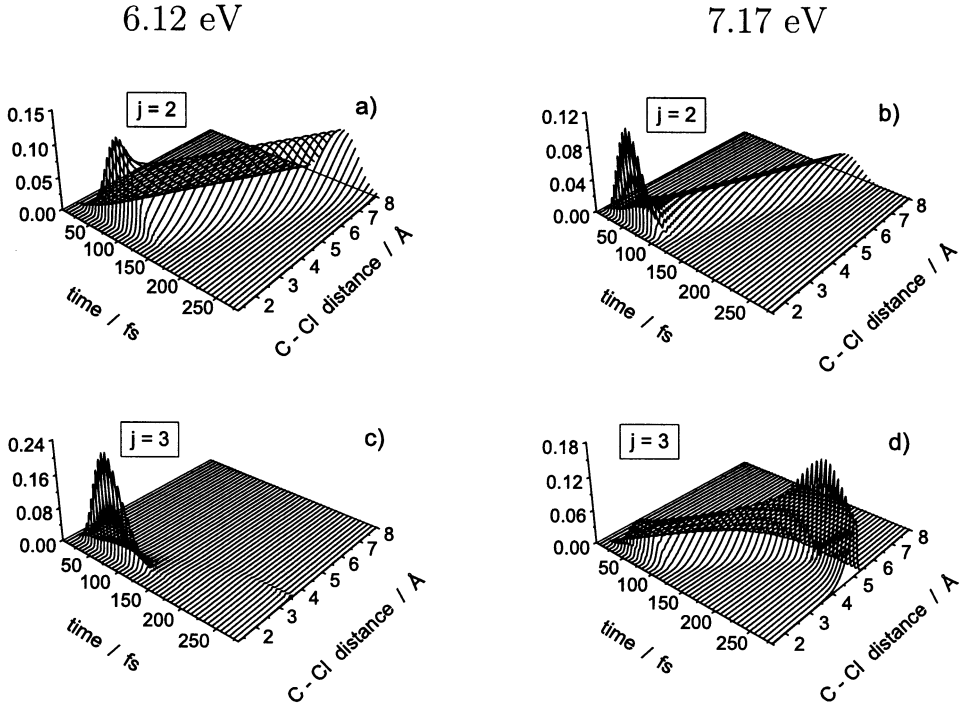

Figure 9. Propagation of one-dimensional wave functions, $|\chi^{d}_{j\epsilon=z}(q_{Cl}, t)|$ on the diabatic potential curves $j = 2$, 3 under irradiation with a pulse of $t_p = 100$ fs duration and photon energy of 6.12 (l.h.s) or 7.17 eV (r.h.s)

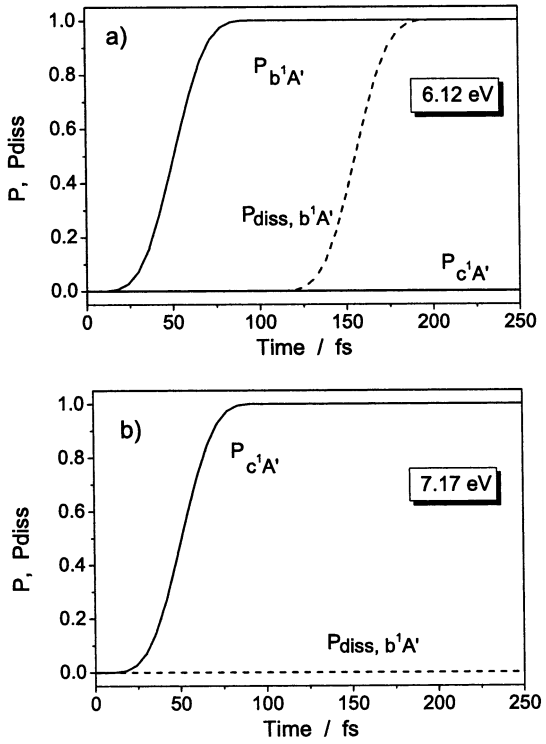

Figure 10. Population dynamics in the C−Br direction on adiabatic potentials b^1A' and c^1A' induced by resonant one-photon excitation. The P stands for normalized excited-state population, $\overline{P_j(t)}/\overline{N}$, where $\overline{N}$ is the asymptotic total excited-state population at $t = 250$ fs. The P_{diss} denotes the normalized probability of dissociation, $\overline{P_{diss,j}(t)}/\overline{N}$. Photon energies are given in the figure. In both cases, the pulse duration is $t_p = 100$ fs and the pulse was centered at 50 fs.

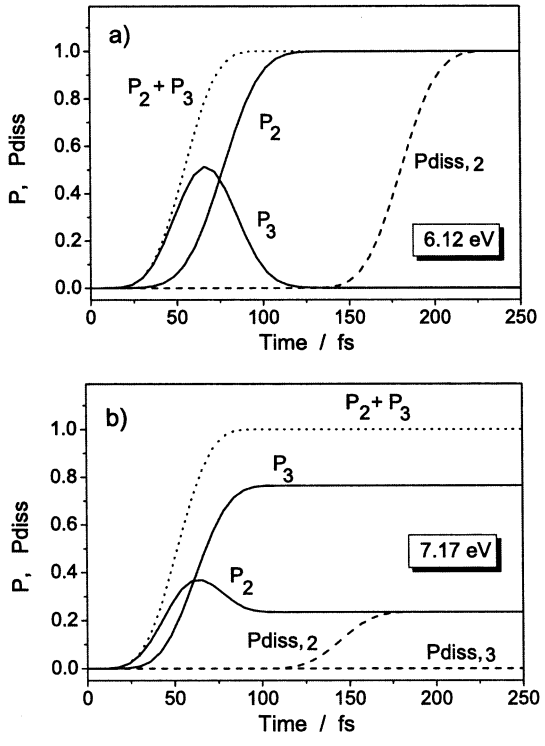

Figure 11. Population dynamics in the C−Cl direction on diabatic potentials induced by resonant one-photon excitation. As in Figure 10, the P and the P_{diss} stand for the normalized excited-state population, $\overline{P_j(t)}/\overline{N}$ and for the normalized probability of dissociation, $\overline{P_{diss,j}(t)}/\overline{N}$, respectively. Photon energies are given in the figure. Pulse parameters are the same as in Figure 10.

coordinate, only the resonant frequency produces significant population transfer (Figure 8a,d). The corresponding wave packet in the b^1A' state dissociates directly (Figure 8a), whereas the wave packet in the c^1A' state shows a first recurrence to the FC region ca. 400 fs after t_0 (Figure 8d). In the Cl dissociation channel, direct excitation to the $j = 2$ diabatic state (cf. Figure 3) with photons of 7.17 eV induces partial dissociation via nonadiabatic effects (Figure 9b). Still the major part of the population remains trapped in $j = 3$ state, showing the first recurrence to the FC region ca. 340 fs after t_0 (Figure 9d).

The corresponding population dynamics and probability of dissociation are shown in Figures 10 and 11 for the C−Br and C−Cl coordinates, respectively. The population is normalized with the asymptotic value of the total excited population after 250 fs. As seen in Figure 10, the excitations are selective with both photon energies. In the C−Cl reaction coordinate, a large population transfer occurs between the diabatic states 2 and 3 (see Figure 11); 80% of the population excited initially to the diabatic state 2 is transferred to the state 3 and only 20% dissociates. The direct dissociation from the b^1A' state in the C−Br direction reaches 36% in less than 100 fs after the excitation ($t_0 = 50$ fs), pointing to a very efficient primary reaction under UV irradiation.

Fitting expression 25 to the nonzero $\overline{P_{\mathrm{diss},j}(t)}$ components and taking into account the center of the laser pulse at $t_0 = 50$ fs, the following dissociation times were obtained: $t_{\mathrm{diss}} = 105$ fs for the C−Br dissociation in state b^1A' in case of 6.12 eV photon energy and $t_{diss} = 130$ and 94.5 fs for dissociation in the C−Cl direction following the excitations by photons of energies 6.12 and 7.17 eV, respectively. The fact that t_{diss} is smaller for the C−Br than for the C−Cl direction indicates that an excitation with photons of 6.12 eV energy is followed by a fission of the C−Br bond rather than the C−Cl one.

4. Concluding Remarks

The photodissociation and electronic spectroscopy of CH_2-BrCl, a model system for halomethanes CH_2XY, has been investigated by means of laser-induced wave packet dynamics propagated on ab initio coupled potentials. Because of the number of avoided crossings and presence of Rydberg states along the reaction path, it is mandatory that the potentials are calculated by means of sophisticated multiconfigurational methods, like MS−CASPT2 which can treat near-degeneracies and Rydberg-valence mixing adequately. Potential energy curves and transition dipole moments for the ground and excited singlet states have been obtained as a function of two coordinates, q_{Br} and q_{Cl}, corresponding to the primary photodissociation pathways of CH_2BrCl. In each reaction coordinate, the lowest singlet excited state, assigned to $n \rightarrow \sigma^*(C-Y)$ transitions (Y = Br and Cl), is predicted to be repulsive for both C−Br and C−Cl eliminations. Accordingly, on the basis of one-dimensional dynamical simulations, one-photon resonance excitation leads to bond breaking in a time scale of about 100 fs. An excitation to the b^1A' state is followed by a direct and fast dissociation of the weaker C−Br bond rather than the fission of the C−Cl one. On the other hand, in the frame of the present one-dimensional model, an excitation to the c^1A' state is partially followed by dissociation of the C−Cl bond because of nonadiabatic dynamics via a $n\sigma^*(C-Br)/n\sigma^*(C-Cl)$ curve crossing; this implies that in higher dimensionality the Cl photofragmentation involves a conical intersection funnel. Higher excited singlet states present very complicated crossing patterns, which offer multiple possibilities for laser control experiments guided by feedback learning algorithms.[58] In view of the challenging task which supposes full understanding of the microscopic mechanism induced by such laser fields, future work should include dynamical simulations in more dimensions as well as additional excited states with their corresponding nonadiabatic couplings.

We have also calculated the vertical excitation energies and corresponding oscillator strengths for the resulting CH_2Br and CH_2Cl radicals, finding a close agreement with the latest available UV spectra and measured absorption cross-sections. The theoretical results indicate that CH_2Br and CH_2Cl spectra possess a single band peaking at 230 and 197 nm, respectively, as suggested by Villenave's[46] and Roussel's[49] flash photolysis experiments. In each case, the dominant excited state corresponds to a $\pi(C-X) \rightarrow \pi^*(C-X)$ transition.

Acknowledgment. We are grateful to Dr. J. Full for his help in the potential diabatization. Financial support from the Deutsche Forschungsgemeinschaft DFG is acknowledged. All quantum chemical calculations have been performed on HP workstations of the Theoretische Chemie group at Freie Universität Berlin.

Note Added after ASAP Posting. This article was released ASAP on 10/24/2002 with minor errors in eqs 6 and 10. The correct version was posted on 10/24/2002.

References and Notes

(1) *Chemistry and Radiation Changes in the Ozone Layer*; Zerefos, C. S., Isaksen, I. S. A., Ziornas, I., Eds.; Kluwer: Dordrecht, The Netherlands, 2001.
(2) Barrie, L. A.; Bottenheim, J. W.; Shnell, R. C.; Crutzen, P. J.; Rassmussen, R. A. *Nature (London)* **1988**, *334*, 138.
(3) Wayne, R. P. *The Chemistry of Atmospheres*; Oxford University Press: New York, 1991.
(4) Vogt, R.; Crutzen, P. J.; Sander, R. *Nature* **1996**, *383*, 327.
(5) Wubbles, D. J.; Jain, A. K.; Patten, K. O.; Connell, P. S. *Atmos. Environ.* **1997**, *32*, 107.
(6) Orkin, V. L.; Khamagonov, V. G.; Guschin, A. G.; Huie, R. E.; Kurylo, M. J. *J. Phys. Chem.* **1997**, *101*, 174.
(7) Bilde, M.; Wallington, T. J.; Ferronato, C.; Orlando, J. J.; Tyndall, G. S.; Estupinan, E.; Haberkorn, S. *J. Phys. Chem. A* **1998**, *102*, 1976.
(8) McGivern, W. S.; Li, R.; Zou, P.; North, S. W. *J. Chem. Phys.* **1999**, *111*, 5771.
(9) Vogt, R.; Sander R.; von Glasow, R.; Crutzen, P. J. *J. Atmos. Chem.* **1999**, *32*, 375.
(10) Zou, P.; McGivern, W. S.; North, S. W. *Phys. Chem. Chem. Phys.* **2000**, *2*, 3785.
(11) Mitchell, R. C.; Simons, J. P. *Discuss. Faraday Soc.* **1967**, *44*, 208.
(12) Butler, L. J.; Hintsa, E. J.; Lee, Y. T. *J. Chem. Phys.* **1986**, *84*, 4104.
(13) Butler, L. J.; Hintsa, E. J.; Lee, Y. T. *J. Chem. Phys.* **1987**, *86*, 2051.
(14) Zhang, J.; Heller, E. J.; Huber, D.; Imre, D. G.; Tannor, D. *J. Chem. Phys.* **1989**, *89*, 3602.
(15) Das, S.; Tannor, D. *J. Chem. Phys.* **1989**, *91*, 2324.
(16) Tzeng, W. B.; Lee, Y. R.; Lin, S. M. *Chem. Phys. Lett.* **1994**, *227*, 467.
(17) Takayanagi, T.; Yokoyama, A. *Bull. Chem. Soc. Jpn.* **1995**, *68*, 2225.
(18) Jung, Y.-J.; Park, M. S.; Kim, Y. S.; Jung, K.-H.; Volpp, H.-R. *J. Chem. Phys.* **1999**, *111*, 4005.
(19) Lee, S.-H.; Jung, Y.-J.; Jung, K.-H. *Chem. Phys.* **2000**, *260*, 143.
(20) Lee, S.-H.; Jung, K.-H. *Chem. Phys. Lett.* **2001**, *350*, 306.
(21) Abrashkevich, D. G.; Shapiro, M.; Brumer, P. *J. Chem. Phys.* **2002**, *116*, 5584.
(22) Damrauer, N. H.; Dietl, C.; Kramert, G. Lee, S.-H.; Jung, K.-H.; Gerber, G. *Eur. Phys. J. D* **2002**, *20*, 71.
(23) Zewail, A. H. *Angw. Chem. Int. Ed.* **2000**, *39*, 2586 (Nobel Lecture).
(24) Zare, R. N. *Science* **1998**, *279*, 1879.
(25) Rabitz, H.; de Vivie-Riedle, R.; Motzkus, M.; Kompa, K. *Science* **2000**, *288*, 824.
(26) For a monography on laser control, see: Rice, S. A.; Zhao, M. *Optical Control of Molecular Dynamics*; Wiley: New York, 2000.
(27) Roeterdink, W. G.; Janssen, M. H. M. *Phys. Chem. Chem. Phys.* **2002**, *4*, 601.
(28) Rozgonyi, T.; Feurer, T.; González, L. *Chem. Phys. Lett.* **2001**, *350*, 155.
(29) Li, Y.; Francisco, J. S. *J. Chem. Phys.* **2001**, *114*, 2879.
(30) Roos, B. O. In *Advances in Chemical Physics; Ab initio Methods in Quantum Chemistry II*; Lawley, K. P., Ed.; Wiley: Chinchester, U.K., 1987; p 399.
(31) Finley, J.; Malmqvist, P.-A.; Roos, B. O.; Serrano-Andrés, L. *Chem. Phys. Lett.* **1998**, *288*, 299.
(32) Andersson, K.; Malmqvist, P.-A.; Roos, B. O. *J. Chem. Phys.* **1992**, *96*, 1218.
(33) Roos, B. O.; Andersson K. *Chem. Phys. Lett.* **1995**, *245*, 215.
(34) Widmark, P.-O.; Malmqvist, P.-A.; Roos, B. O. *Theor. Chim. Acta* **1990**, *77*, 291.
(35) Barandiarán, Z.; Seijo, L. *Can. J. Chem.* **1992**, *70*, 409.
(36) Kaufmann, K.; Baumeister, W.; Jungen, M. *J. Phys. B: At. Mol. Opt. Phys.* **1989**, *22*, 2223.

(37) Malmqvist, P.-A.; Roos, B. O. *Chem. Phys. Lett.* **1989**, *155*, 189.
(38) Andersson, K.; et al., *MOLCAS* 5.0; University of Lund: Lund, Sweden, 2000.
(39) Baer, M. *Chem. Phys. Lett.* **1975**, *35*, 112.
(40) Smith, F. T. *Phys. Rev.* **1969**, *179*, 111.
(41) Feit, M. D.; Fleck, J. A.; Steiger, A. *J. Comput. Phys.* **1982**, *47*, 412. Fleck, J. A.; Morris, J. R.; Feit, M. D.; *Appl. Phys.* **1976**, *10*, 1929.
(42) Kosloff, D.; Kosloff, R. *J. Comput. Chem.* **1982**, *52*, 35.
(43) Marston, C.; Balint-Kurti, G. *J. Chem. Phys.* **1989**, *91*, 3571.
(44) Saalfrank, P. *Chem. Phys.* **1995**, *193*, 119.
(45) Finger, K.; Daniel, C.; Saalfrank, P.; Schmidt, B. *J. Phys. Chem.* **1996**, *100*, 3368.
(46) Villenave, E.; Lesclaux, R. *Chem. Phys. Lett.* **1995**, *236*, 376.
(47) Nielsen, O. J.; Munk, J.; Locke, G.; Wallington, T. J. *J. Phys. Chem.* **1991**, *95*, 8714.
(48) Chong, C. K.; Zheng, X.; Phillips, D. L. *Chem. Phys. Lett.* **2000**, *328*, 113.
(49) Roussel, P. B.; Lightfoot, P. D.; Caralp, F.; Catoire, V.; Lesclaux, R.; Forst W. *J. Chem. Soc. Faraday Trans.* **1991**, *87*, 2367.
(50) Andrews, L.; Dyke, J. M.; Jonathat, N.; Keddar, N.; Morris, A.; Ridha, A. *Chem. Phys. Lett.* **1983**, *97*, 89.
(51) *Handbook of Chemistry and Physics*, 76th ed.; Linde, D. R., Ed.; CRC Press: Boca Raton, FL, 1996.
(52) Kubodera, S.; Wisoff, P. J.; Sauerbrey, R. *J. Chem. Phys.* **1990**, *92*, 5867.
(53) Hachey, M. R. J.; Daniel, C. *Inorg. Chem.* **1998**, *37*, 1387.
(54) For consistency, the dissociating energies were calculated using nine roots in the equilibrium geometry.
(55) The dissociation energy computed between C−Br = 10 Å and C−Br = 1.933 Å is 3.14 eV. This value is more reliable than the 3.22 eV because the active space at C−Br = 50 Å conforms different excitations than the ones present at equilibrium.
(56) Daniel, C.; Full, J.; González, L.; Kaposta, C.; Krenz, M.; Lupulescu, C.; Manz, J.; Minemoto, S.; Oppel, M.; Francisco, P. R.; Vajda, S.; Wöste, L. *Chem. Phys.* **2001**, *267*, 247.
(57) Schinke, R. *Photodissociation dynamics*; University Press: Cambridge, 1993.
(58) Judson, R. S.; Rabitz, H. *Phys. Rev. Lett.* **1992**, *68*, 1500.